

DTI at long diffusion time improves fiber tracking

Swati Rane^{a,b}, Govind Nair^b and Timothy Q. Duong^{c,d,e*}

While diffusion-tensor-imaging tractography provides remarkable *in vivo* anatomical connectivity of the central nervous system, the majority of DTI studies to date are predominantly limited to tracking large white-matter fibers. This study investigated DTI tractography using long diffusion time (t_{diff}) to improve tracking of thinner fibers in fixed rhesus monkey brains. Stimulated Echo Acquisition Mode (STEAM) sequence on a 3T Siemens TRIO was modified to include a diffusion module. DTI was acquired using STEAM with t_{diff} of 48 and 192 ms with matched signal-to-noise ratios (SNR). Comparisons were also made with the conventional double-spin echo (DSE) at a short t_{diff} of 45 ms. Not only did the fractional anisotropy increase significantly with the use of long diffusion time, but directional entropy measures indicated that there was an increased coherence amongst neighboring tensors. Further, the magnitude of the major eigenvector was larger at the $t_{\text{diff}} = 192$ ms as compared to the short t_{diff} . Probabilistic connectivity maps at long t_{diff} showed larger areas of connectivity with the use of long diffusion time, which traversed deeper into areas of low anisotropy. With tractography, it was found that the length of the fibers, increased by almost 10% in the callosal fibers that branch into the paracentral gyrus, the precentral gyrus and the post central gyrus. A similar increase of about 20% was observed in the fibers of the internal capsule. These findings offer encouraging data that DTI at long diffusion time could improve tract tracing of small fibers in areas of low fractional anisotropy (FA), such as at the interfaces of white matter and grey matter. Copyright © 2010 John Wiley & Sons, Ltd.

Keywords: diffusion tensor imaging; STEAM sequence; rhesus macaques; cross-terms; formalin fixation; fractional anisotropy; white matter tracking

INTRODUCTION

Diffusion tensor imaging (DTI) (1,2) contrast in biological systems arises from water movement in the presence of barriers (such as cell membranes of axons and oligodendrocytes) that hinder water diffusion more in some orientations than others. DTI has been widely used to map whole-brain anatomical connectivity in a totally non-invasive fashion (3). This is in marked contrast to histological tracing techniques (invasive) where radioactive or fluorescent tracers are focally injected to track regional connections over a few synapses (limited coverage), precluding whole-brain, longitudinal and *in vivo* studies and human applications.

The majority of DTI tractography studies to date are limited to tracking large white-matter fibers. Novel approaches such as multiple high b-value DTI (4), high angular resolution DTI (HARD) (5) and Q-ball imaging (6) are being actively explored to improve diffusion-based tractography. A unique feature of many of these approaches is that, in contrast to conventional DTI tractography, they do not assume Gaussian diffusion (6). Yoshiura *et al.* measured DTI indices using very high values (500 to 5000 s/mm²) (36) and showed that, as the b-value increased, apparent diffusion coefficient (ADC) decreased in both the gray and white matter. They also found that non-monoexponential diffusion signal decay was more prominent in white matter than in gray matter. Surprisingly, there was no significant change in the relation of the b-value to the FA maps. High b-value appears to have a dissociating effect on gray and white matter in DWIs. Ronen *et al.* performed DTI tractography using multi-exponential decays. By decomposing into slow and fast diffusion tensors and compared with conventional DTI data (4),

they reported that fibers generated on the basis of the slow diffusion component appear to follow the vertical fibers in gray matter. DTI of the slow component may provide a way for increasing the sensitivity to anisotropic structures in cortical gray matter. While these novel approaches are promising, they

* Correspondence to: T. Duong, Research Imaging Institute, 8403 Floyd Curl Dr, San Antonio, TX 78229, USA.
E-mail: duongt@uthscsa.edu

a S. Rane
Biomedical Engineering, Georgia Institute of Technology, GA, USA

b S. Rane, G. Nair
Emory University, Atlanta, GA, USA

c T. Q. Duong
Research Imaging Institute, Departments of Ophthalmology, Radiology, and Physiology, University of Texas Health Science Center, San Antonio, TX, USA

d T. Q. Duong
South Texas Veterans Health Care System, San Antonio, TX, USA

e T. Q. Duong
Southwest National Primate Research Center, San Antonio, TX, USA

Contract/grant sponsor: NIH; contract/grant number: R01NS45879.

Contract/grant sponsor: The Center for Behavioral Neuroscience; contract/grant number: NSF, IBN-9876754.

Abbreviations used: ADC, apparent diffusion coefficient; DTI, diffusion tensor imaging; HARD, high angular resolution DTI; FA, fractional anisotropy; ROI, region of interest; STEAM, Stimulated-Echo-Acquisition-Mode dual spin-echo (DSE); SNR, signal-to-noise ratio.

require very large b -values that are not readily achievable on clinical scanners due to gradient strength limitations. They are also generally more difficult to implement compared to conventional DTI techniques.

The root-mean-squared (7,8) displacement in diffusion measurement is dependent on diffusion time (t_{diff}). For a t_{diff} of 20 ms, the rms displacement is $\approx 10 \mu\text{m}$ *in vivo* (7,8), on the order of cell sizes in the brain, and diffusion is largely sensitive to restriction by cell membranes and subcellular organelles. At $t_{\text{diff}} \approx 200$ ms, the rms displacement is $\approx 32 \mu\text{m}$, substantially larger than the average cell sizes, and diffusion is also sensitive to restriction in the extracellular spaces along fiber tracts. Indeed, the ADC of water *in vivo* has been shown to be dependent on t_{diff} , with ADC decreasing rapidly for t_{diff} from 2 to 15 ms and gradually for t_{diff} greater than 20 ms (9–11). ADC in human brains is diffusion-time dependent (12). Fractional anisotropy (FA) at longer t_{diff} has been reported to be more sensitive to changes in myelin-deficient mice (13). These findings suggest that DTI at long diffusion time could improve tractography. DTI studies to date employed relatively short t_{diff} to minimize signal loss due to T2 decay and DTI tractography at long t_{diff} has not been reported.

The goal of this study was to determine whether DTI at long t_{diff} improves tracking of thinner fibers. To overcome T2 signal loss associated with long t_{diff} measurements, Stimulated-Echo-Acquisition-Mode (STEAM) sequence (14,15) was modified to include a diffusion module to sample 30 diffusion directions on a 3T Siemens TRIO. DTI tractography was performed with short (48 ms) and long (192 ms) diffusion time on post-mortem fixed monkey brains. Standard dual spin-echo (DSE) (16) DTI data were also acquired on the same monkey brains in the same setting for comparison in order to ascertain that the improvement was indeed due to the application of the longer diffusion time and not due to a different sequence. FA, tensor-field plots, connectivity maps based on entropy minimization (17) and deterministic fiber tractography using line propagation (3) were compared among the three methods with matched signal-to-noise ratio (SNR) and identical statistical thresholds.

METHODS

Phantom experiments

Cross-term interactions among diffusion and imaging gradients in STEAM acquisition at long t_{diff} can be significant (18–20) and can adversely affect DTI measurements. While cross-term interactions could be calculated to derive the exact b values (19,21), geometric averaging approach was used to remove cross-term bias (19,22) without evaluating the exact b -values. This involved acquiring two DTI data sets in which two DWI were acquired in the same diffusion gradients but with opposite gradient polarities. The two images are multiplied on a pixel by pixel basis. The square root of the product results in an image with substantially reduced cross-term effects. Phantom studies were performed to evaluate and confirm the validity of this approach. A phantom, 45 mm in diameter, made of 0.5 M ^1H -mannitol dissolved in dimethylsulfoxide (DMSO), was chosen because the ADC of mannitol in DMSO (as opposed to water phantom) is more similar to water ADC in fixed brain. This allows the use of identical b -values and imaging protocols for both phantom and brain studies.

Fixed monkey brains

Eight measurements were made on four rhesus monkey brains fixed with 4% formalin. Brains were perfused-fixed and stored in formalin for a maximum of 5 days before MRI. During imaging, the sample was submerged in water to minimize susceptibility on the surface of the brain. The strong bulk water signal along the sharp edges of the container, however, gave rise to Gibbs ringing artifacts. A small amount of MION (0.018 mg/mL) was added to eliminate Gibbs ringing. The large MION particles could not enter the interstitial space of the brain tissue, as confirmed by the absence of degradation of echo-planar images and SNRs acquired up to a week after the MION addition.

MRI methods

MRI studies were performed on a Siemens 3T Trio clinical scanner (Siemens AG, Erlangen, Germany). All samples were scanned at room temperature. T1-weighted images were acquired using conventional gradient-echo acquisition, with TR = 4000 ms, flip angle = 25° , TE = 7.7 ms, FOV = 70×70 mm, matrix size = 128×128 , and slice thickness = 2 mm.

DTI data were acquired with a 16-shot STEAM (14,15) EPI sequence with TR = 1500 ms, TE = 80 ms, 30 diffusion directions with $b = 1700 \text{ s/mm}^2$ and a single $b = 0 \text{ s/mm}^2$ acquisition, FOV = 70×70 mm, matrix size = 128×128 , 3 slices, slice thickness = 2 mm, and $\delta = 21$ ms. Data were acquired at two mixing times (TM) of 25 and 169 ms, which corresponded to t_{diff} of 48 and 192 ms, respectively. The corresponding numbers of averages were 34 and 70, respectively, chosen so as to match SNR (determined as the ratio of an ROI intensity of the WM in the brain to the standard deviation of ROI intensity outside the brain). These two methods are hereby referred to as STEAM-48 ms and STEAM-192 ms. The b value of 1700 s/mm^2 was used instead of the typical 1000 s/mm^2 *in vivo* because fixation decreases ADC value. Note that the TE at long t_{diff} could be substantially shortened (to ~ 63 ms) to achieve the same b value which should reduce number of averaging needed. In this study, the same TE was employed for both long and short t_{diff} to avoid potential bias due to different T2 weighting in the WM and GM.

For comparison, DTI was also acquired using the standard double spin-echo (DSE) sequence (16) in the same imaging sessions with similar parameters except that the TE was 104 ms which was the minimum achievable value for the experimental parameters. The effective t_{diff} for DSE was 45 ms. The number of averages, chosen to match SNR of the STEAM acquisitions, was 48. Acquisitions of the three protocols were interleaved and randomized to minimize the effect of potential systematic drifts. The total imaging time for the STEAM-48 ms was 14.16 h. For the DSE sequence the time was 20 hours while for the STEAM-192 ms sequence, it was 29.16 h.

Data analysis

Anisotropy calculations

All analyses were performed using codes written in MATLAB[®] (Mathworks, Natick, MA) unless otherwise specified. FA maps were computed (1,23). White matter (WM) and gray matter (GM) pixels were separated using intensity-based segmentation on T1-weighted images and the mean WM and GM FA were calculated.

Spherical (CS), planar (CP) and linear (CL) anisotropy measures were calculated and plotted on the barycentric coordinate system (three-phase plot) (24)

$$x = \frac{1 - CP + CL}{\sqrt{3}}, \text{ and } y = 1 - CP - CL. \quad (1)$$

where $CS = \frac{\lambda_3}{3(\lambda)}$, $CP = \frac{2(\lambda_2 - \lambda_3)}{3(\lambda)}$, $CL = \frac{\lambda_1 - \lambda_2}{3(\lambda)}$, and λ_1 , λ_2 , and λ_3 are the eigen-values of the 3×3 diffusion tensor matrix, with $\langle \lambda \rangle = \frac{\lambda_1 + \lambda_2 + \lambda_3}{3}$. x and y are co-ordinates on the three-phase plot where isotropy is represented at the apex of the triangle and the left and right vertices correspond to linear and planar anisotropy respectively. The three-phase plot provides a convenient way to study the trend in anisotropy with increasing t_{diff} .

Directional entropy

The tensor-field map was examined for tensor orientations. Long diffusion time could emphasize the dominant fiber in the voxels that comprise of multiple sparse fiber bundles. If these tensors indeed, represented an underlying fiber tract or a continuation of a fiber branch, then the tensors in the neighboring voxels would have similar orientations, i.e. the principal eigenvectors would be co-linear. Such co-linearity would then increase with increase in diffusion time. In order to measure this increase, directional entropy (DE) (26) was used.

For this purpose, a sphere was broken into many triangular faces. Each face was represented by a vector starting from the origin of the sphere and the centroid of the triangular face. Thus, discrete angular orientations, corresponding to each triangular face, were obtained. The principal eigenvectors obtained using DTI were then binned into these discrete vectors. The binning was determined on the basis of the dot product between the principal eigenvector and each discrete vector. The principal eigenvectors was binned into that angular orientation vector which produced the highest value for the dot product. This provided a distribution of the different orientations along a fiber tract. The probability of a tensor direction was evaluated from this distribution and then entropy for the given region of interest along a probable fiber tract was calculated for all three methods and compared. Since only three slices were acquired near the central sulcus, there were two prominent fiber tracts and their branches that could be delineated; the corpus callosum (CC) and the internal capsule (IC).

The value of DE depends on the number of triangular faces used to bin the tensor orientations. For this study, 60, 128, 160, 196 and 320 faces were obtained. It was found that the DE did not change significantly when the number of faces was greater than 160. This study triangulated the sphere into 192 faces to ensure as little variance in entropy as possible due to the binning process.

DTI tensor-field map and connectivity

Front marching algorithm (17) was used to determine the probabilistic connectivity maps in the imaged brain volume. The rate at which the connectivity front propagates from one voxel at location r' to another voxel at r depends on the co-linearity of the principal eigenvector $\varepsilon_1(r)$ amongst the neighbors and the direction in which the front continues to evolve. The rate function employed in this study (17) was

$$f = \frac{1}{(1 - \min(|\varepsilon_1(r) \cdot n(r)|, |\varepsilon_1(r) \cdot \varepsilon_1(r')|))}, \quad (2)$$

where $n(r)$ is the unit vector normal to the front and determines the spread of the front. For comparison, identical cut-off thresholds (0.5 of the maximum value of probabilistic connectivity obtained with equation (2)) were used for all three methods to derive connectivity maps.

DTI tractography

Fiber tracking was performed using DTI Studio v2.4 (27). A FA threshold < 0.1 and a turning angle $> 65^\circ$ were used as termination criteria for fiber propagation for all three methods. DTI Studio v2.4 was also used to calculate the fiber lengths. Lowering the threshold increases the sensitivity to the random fibers and consequently affects the calculation of the fiber lengths. Nonetheless, the trend of increase in fiber length using STEAM192 was still observed at the lowered threshold.

All values in text and on graphs are reported as mean \pm SD. Statistical testing utilized unpaired Student t -test with $p < 0.05$ taken as reaching statistical significance.

RESULTS

Phantom studies

ADC of the ^1H -mannitol phantom measured along the phase-encode direction was $(0.39 \pm 0.01) \times 10^{-3} \text{ mm}^2/\text{s}$ ($n = 8$). ADC along the phase-encoding direction was used as reference for the other two principal directions. Before geometric averaging, ADC values among the three principal axes differed from each other up to $8.1 \pm 1.2\%$ for STEAM-48 ms and $16.7 \pm 1.8\%$ for STEAM-192 ms. After correction, ADC values among the three principal axes differed only up to $3.7 \pm 1.7\%$ for STEAM-48 ms and $6.6 \pm 3.4\%$ for STEAM-192 ms. As expected, ADC along the phase-encoding direction were not statistically different between before and after correction, consistent with the notion that cross-terms were minimal along the phase-encode direction. For DSE, ADC values among the three principal axes differed up to $5.4 \pm 3.9\%$ and no correction was applied. Smaller cross terms in the DSE is likely due to the use of two balancing 180° pulses.

Fractional anisotropy

For all comparisons, SNR among the three methods were matched. Figure 1 shows the FA comparisons among DSE, STEAM-48 ms and STEAM-192 ms of fixed monkey brains. Only WM FA of STEAM-192 ms were statistically different ($p < 0.05$) from those of STEAM-48 ms and DSE. Indeed, WM FA of STEAM-192 ms were larger than that of STEAM-48 ms by $11.5 \pm 5.0\%$ and of DSE by $11.2 \pm 5.0\%$.

The ADC values by STEAM-48 ms, STEAM-192 ms, and DSE were, respectively, $0.18 \pm 0.012 \times 10^{-3} \text{ mm}^2/\text{s}$, $0.16 \pm 0.012 \times 10^{-3} \text{ mm}^2/\text{s}$ and $0.16 \pm 0.012 \times 10^{-3} \text{ mm}^2/\text{s}$ in WM, and $0.26 \pm 0.037 \times 10^{-3} \text{ mm}^2/\text{s}$, $0.26 \pm 0.031 \times 10^{-3} \text{ mm}^2/\text{s}$ and $0.25 \pm 0.028 \times 10^{-3} \text{ mm}^2/\text{s}$ in GM. The ADC obtained with the DSE sequence at a t_{diff} value of 45 ms is similar to that obtained by STEAM-192 ms while the STEAM-48 ms calculates a higher ADC value than STEAM-192 ms. Parallel and perpendicular diffusivities normalized by the trace ADC values were calculated and these values are shown in Table 1.

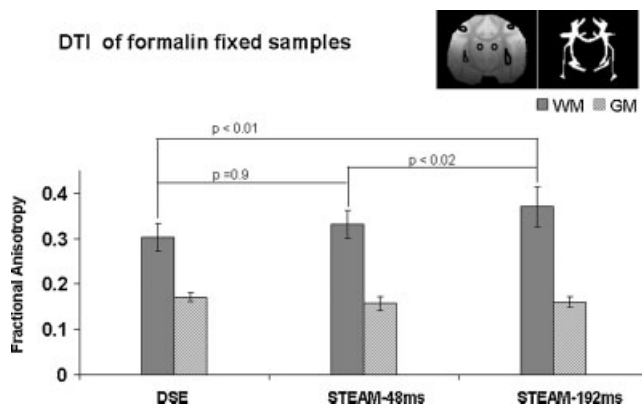


Figure 1. Fractional anisotropy (FA) of fixed rhesus monkey brains acquired using double-spin echo (DSE) with diffusion time = 45 ms, STEAM with diffusion time = 48 (STEAM-48 ms) and 192 ms (STEAM-192 ms). White matter (WM) and gray matter (GM) were segmented based on T1-weighted images. Inset A shows GM ROI and Inset B shows the WM mask used in the generated the FA plots.

Table 1. Measures of parallel diffusivity ($D_{||}$) and perpendicular diffusivity (D_{\perp}), normalized by the ADC. The ratio $D_{||}/D_{\perp}$ increased by approximately 5.7% with STEAM-192 ms as compared to DSE and STEAM-48 ms

	DSE	STEAM-48 ms	STEAM-192 ms
$D_{ }$	0.432 ± 0.017	0.436 ± 0.019	0.456 ± 0.018
D_{\perp}	0.283 ± 0.012	0.284 ± 0.019	0.281 ± 0.017
$D_{ }/D_{\perp}$	1.526 ± 0.016	1.535 ± 0.018	1.622 ± 0.016

Directional Entropy

The directional entropy was evaluated along the callosal fiber tract and the internal capsule to determine if the neighboring tensors were more co-linear at long t_{diff} . The values of DE are

depicted in Table 2. In comparison to STEAM-48 ms, the DE obtained by STEAM192 in the CC and IC was lower by $17.3 \pm 6.3\%$ and $10.5 \pm 1.2\%$ ($p < 0.05$) respectively. The decrease in DE with respect to DSE was $18.1 \pm 7.2\%$ in the CC and $8.4 \pm 1.3\%$ in the IC ($p < 0.05$). In addition Table 2 also shows the values of CL, CP, CS and FA in the same region.

Tensor and tractography

Tensor-field maps were calculated for the three methods with matched SNR (DSE SNR: 36.5, STEAM-48 ms SNR: 33.9, STEAM-192 ms SNR: 34.6). STEAM-192 ms showed substantially larger magnitudes of the principal eigenvectors (Fig. 2) and improved coherence amongst adjacent tensors compared to those of STEAM-48 ms and DSE. Diffusion entropy indices were 2.03, 2.10 and 1.96 for DSE, STEAM-48 ms and STEAM-192 ms, respectively, for the region shown in the figure. The decreased entropy indicated that STEAM-192 ms had a higher degree of similarity in tensor orientation among neighboring voxels.

The three-phase plots of spherical, linear and planar anisotropy (Fig. 3) showed STEAM-192 ms had the highest linear anisotropy among the three methods with matched SNR. Planar diffusion was similar among the three methods.

Connectivity maps (Fig. 4) were constructed using the fast marching method. With the same cut-off statistical thresholds for all three methods for comparison, STEAM-192 ms revealed more extensive connectivity in the low FA regions compared to DSE and STEAM-48 ms. This was particularly evident in the regions of the post central gyrus (vertical arrows). DSE, on the other hand, showed less connectivity in this region. All three methods showed connectivity to large callosal fibers and the cortico-pontine/cortico-bulbar fibers as expected.

Fiber tracking was performed on multiple selected regions of interest, including the corpus callosum, internal capsule and external capsule (Fig. 5). The callosal fiber tracts extended further toward the cortical surface with STEAM-192 ms into the post central gyrus. Cortico-striatal and corticospinal fibers in the posterior internal capsule (white arrows) were significantly longer in STEAM-192 ms compared to DSE and STEAM-48 ms. Analysis of

Table 2. CL, CP, CS, FA and DE measures in the corpus callosum and the internal capsule for the DSE, STEAM-48 ms and STEAM-192 ms acquisitions

Region	Method	CL	CP	CS	FA	DE	p (DSE vs STEAM-192 ms)	p (STEAM-48 ms vs STEAM-192 ms)
Corpus callosum	DSE	0.35 ± 0.09	0.18 ± 0.08	0.47 ± 0.10	0.32 ± 0.07	3.19 ± 0.10		
	STEAM-48 ms	0.35 ± 0.08	0.18 ± 0.09	0.47 ± 0.09	0.33 ± 0.06	3.23 ± 0.11		
	STEAM-192 ms	0.37 ± 0.09	0.19 ± 0.09	0.44 ± 0.09	0.36 ± 0.07	2.64 ± 0.13		
							0.03	0.02
							0.261	0.223
							< 0.01	< 0.01
Internal capsule	DSE	0.41 ± 0.09	0.20 ± 0.08	0.39 ± 0.10	0.49 ± 0.10	2.44 ± 0.43		
	STEAM-48 ms	0.42 ± 0.09	0.19 ± 0.07	0.39 ± 0.08	0.50 ± 0.11	2.38 ± 0.45		
	STEAM-192 ms	0.45 ± 0.09	0.19 ± 0.09	0.36 ± 0.09	0.56 ± 0.09	2.19 ± 0.43		
							< 0.01	< 0.01
							0.292	0.246
							< 0.01	< 0.01

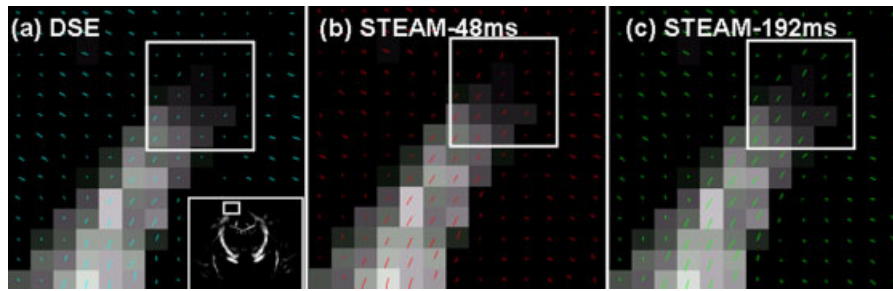


Figure 2. Tensor-field maps overlaid on the fractional anisotropy (FA) maps a fixed monkey brain obtained using (a) DSE, (b) STEAM-48 ms, and (c) STEAM-192 ms. Inset: FA map showing the expanded ROI.

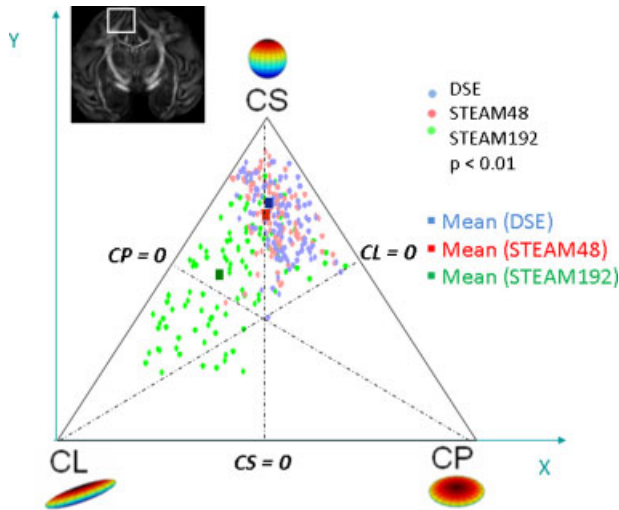


Figure 3. Three-phase plot of the spherical (CS), planar (CP) and linear (CL) anisotropy fixed rhesus monkey brain acquired using DSE, STEAM-48 ms and STEAM-192 ms. Data were obtained from the ROI shown in the inset.

the group-averaged data indicated that the callosal fibers with STEAM-192 ms were $13.9 \pm 0.7\%$ longer than DSE and $14.6 \pm 0.8\%$ longer than STEAM-48 ms. The tracts in the internal capsule with STEAM-192 ms were $21.2 \pm 1.1\%$ longer than DSE

and $24.8 \pm 1.3\%$ longer than STEAM-48 ms. The number of fibers traced were however not statistically different.

DISCUSSION

The major findings of this study are: DTI at longer t_{diff} increases linear anisotropy, yielding increased tensor magnitude and tensor coherence amongst adjacent voxels, and DTI at long t_{diff} improves connectivity and tractography outcome compared to DTI at short t_{diff} .

Technical considerations

Geometric averaging

Geometric averaging is a simple and effective method to minimize diffusion cross-term interactions (19,22) and, thus, directional bias in DTI data. A drawback of geometric averaging is that the scan time is doubled but this is not an issue if signal averaging is needed. In principle, noise propagation of geometric averaging is worse than arithmetic averaging. The SNR of the geometric averaging in this study was slightly lower (by 5% in this study) than arithmetic averaging. Another method of cross-term correction is to experimentally determine a correction factor for each gradient direction for specific protocol parameters such that the same effective b-value can be achieved for different diffusion directions on a uniform phantom (13).

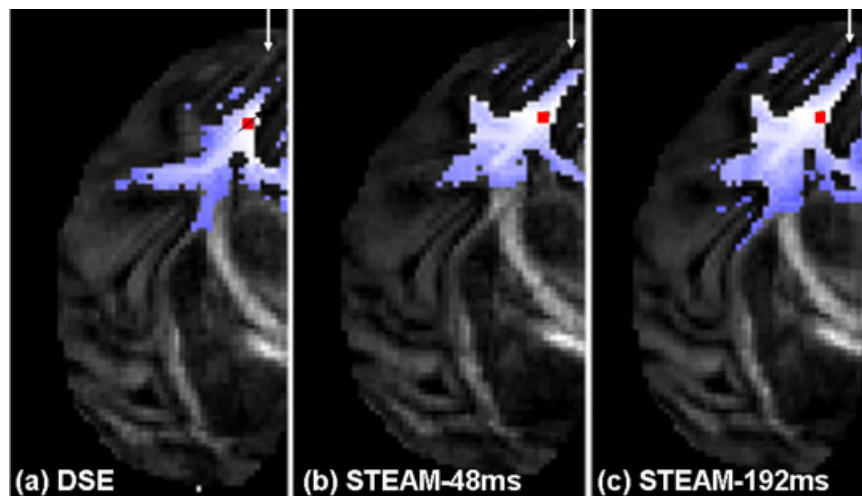


Figure 4. DTI connectivity maps of a fixed rhesus monkey brain obtained using (a) DSE, (b) STEAM-48 ms, and (c) STEAM-192 ms. The red square and the arrow indicate the seed and orientation of the principal eigenvector in the seed.

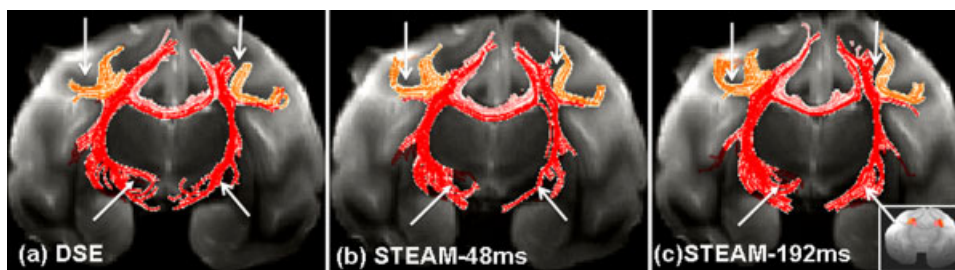


Figure 5. 3D DTI tractography of a fixed rhesus monkey brain acquired using DSE, STEAM-48 ms, and STEAM-192 ms. The seed employed is shown in the inset. The pink traces indicate callosal fibers, orange traces indicate association fibers and red traces indicate cortico-pontine/cortico-bulbar tracts. White arrows indicate the longer fibers delineated by STEAM-192 ms compared to DSE and STEAM-48 ms.

SNR

DTI using spin-echo acquisition at long t_{diff} requires long echo time and is thus not commonly used due to T2 signal loss. The modified STEAM sequence allows long t_{diff} measurements by placing the magnetization along the Z direction during the TM period where signal loss is governed by T1 as opposed to T2 processes. Given that T1 is substantially longer than T2, signal loss at longer t_{diff} is less for STEAM acquisition compared to DSE for the same t_{diff} . The drawback of the STEAM sequence is that only half of the magnetization is retained. Such SNR loss was compensated by a shorter echo time achievable by STEAM. Indeed, STEAM-48 ms and DSE yielded a similar SNR per unit time. STEAM-192 ms had a slightly poorer SNR than DSE and thus required more averaging. We anticipate that STEAM acquisition will be more favorable *in vivo* because of the longer *in vivo* T1 compared to fixed brain. Note that, TE of the long t_{diff} protocol herein was not minimized as described in the Methods section. Future studies can utilize minimal TE for long t_{diff} DTI to improve SNR.

Different spin populations

Comparison between STEAM and DSE DTI data needs to be made with caution because they could have different T1 and T2 weighting. Each voxel of the DSE acquisition has larger contribution of the longer T2 water species, whereas each voxel of the STEAM acquisition at long t_{diff} has larger contribution from longer T1 water species. Indeed, FA, ADC, λ_2 and λ_3 were significantly different ($p < 0.05$) between short (60 ms) and long (80 ms) TE acquired using STEAM-192 ms. Nonetheless, these effects are unlikely to alter the fiber tracking outcome and the overall conclusions of this study.

Effect of formalin

Fixation prevents tissue degradation allowing studies to be performed over hours to days to improve high spatial resolution and to study multiple protocols in a single setting for robust comparison. Fractional anisotropy in fixed brains and *in vivo* studies are comparable (28–30). However, FA is affected by fixation and is dependent on the length of fixation duration until the tissue is completely fixed (31). Formalin fixation causes protein cross-linking and reduces ADC and T2 (32,33). Over the duration of the DTI measurements and the relatively short time after fixation that the samples were studied, 4% formalin adequately preserves tissue integrity. Importantly, acquisitions of the three methods were interleaved and, thus, minor tissue degradation over the course of measurements, if existed, should not affect our overall conclusions.

DTI at long t_{diff}

DTI at long t_{diff} generally increases WM FA while FA in the GM is unaltered. FA increase *per se* at long t_{diff} may not necessarily improve contrasts between WM and GM if both were to increase proportionally. Tensor field maps, probabilistic connectivity and fiber tracking were analyzed using the same cut-off thresholds and at similar SNR values. Increased tensor magnitude and increased coherence of the tensor directions amongst the neighboring voxels in regions of lower anisotropy at long t_{diff} further support the notion that DTI at long t_{diff} improved sensitivity towards thin fibers. Moreover, STEAM-192 ms showed considerable improvements in tracking smaller fibers and more extensive fiber connectivity with the fast marching technique. For example, the callosal fiber tracts in STEAM-192 ms extended further into the WM-GM interfaces toward the cortical surface than the other two methods. Fiber length measurements further corroborated that long t_{diff} indeed improved tracking of thinner fibers. Our findings are in good agreement with long t_{diff} DTI measurements in *ex vivo* calf tongue and heart (34) and *in vivo* mouse brain (13) although fiber tracking was not performed in those studies. A possible explanation that long t_{diff} improves DTI tractography is that water molecules improve sampling of the anisotropic media, and thus increases DTI sensitivity in regions of low diffusion anisotropy. The exact mechanism of improved DTI tractography at long t_{diff} remains to be investigated. A possible mechanism is that the rms displacement with t_{diff} of ~ 200 ms is substantially larger than the average cell sizes and, thus, DTI at long t_{diff} has an increased sensitivity to water movement in the extracellular spaces along the fiber tracts where it is less restricted by cell membranes, compared to DTI at short t_{diff} . Water exchange could become significant. However, the mean intracellular water resident time in the brain has been estimated to be on the order of 600 ms (38). Consequently, with t_{diff} of 200 ms, water exchange effect will be negligible.

Future perspective

Long t_{diff} acquisition can also be combined with other methods (such as multiple high b values) to further improve tractography. Long t_{diff} DTI can also be combined with fiber tracking methods, such as advanced fast marching methods (37), which makes use of the CL measure of anisotropy to detect the presence of branching fiber bundles in a given voxel, and the complete diffusion tensor information. If indeed the diffusion space is better probed at long t_{diff} , the resulting eigen analysis would better delineate branching fibers.

The total acquisition times of our fixed brain studies herein were long because of the short T1, T2 and ADC as well as the desire to compare the three protocols in the same subject. *In vivo* T1, T2 and ADC are substantially larger. This should shorten data acquisition time. The number EPI segmentations could also be reduced. Moreover, future DTI studies can utilize a single long t_{diff} DTI protocol and with minimal echo time once it is proven favorable. Our preliminary *in vivo* data indicate that DTI acquisition time of a single long t_{diff} is comparable to typical DTI measurements.

In conclusion, this study provides multiple corroborative evidences that DTI tractography at long diffusion time improves tracking of smaller fibers in regions of low fractional anisotropy. We predict that *in vivo* DTI at longer t_{diff} could improve tractography. If confirmed, this approach could have positive impact on DTI tractography studies.

Acknowledgements

The authors would like to thank Dr Teijun Zhao for help with the STEAM sequence and Drs Xiaodong Zhang, Shawn Ma, Yoji Tanaka, and Chris Edmonds for helpful discussion and assistance. This work was supported by NIH (R01NS45879) and the Center for Behavioral Neuroscience (NSF, IBN-9876754).

REFERENCES

- Basser PJ, Mattiello J, LeBihan D. Estimation of the effective self-diffusion tensor from the NMR spin echo. *J. Magn. Reson. B* 1994; 103(3): 247–254.
- Basser PJ, Mattiello J, LeBihan D. MR diffusion tensor spectroscopy and imaging. *Biophys. J.* 1994; 66(1): 259–267.
- Mori S, van Zijl PC. Fiber tracking: principals and strategies – a technical review. *NMR Biomed.* 2002; 15(7–8): 468–480.
- Ronen I, Kim K-H, Garwood M, Ugurbil K, Kim D-S. Conventional DTI vs. slow and fast diffusion tensors in cat visual cortex. *Magn. Reson. Med.* 2003; 49: 785–790.
- Tuch D, Reese TG, Wiegall MR, Makris N, Belliveau JW, Wedeen VJ. High Angular Resolution Diffusion imaging Reveals Intravoxel White Matter Fiber Heterogeneity. *Magn. Reson. Med.* 2002; 48: 6.
- Tuch D. Q-ball imaging. *Magn. Reson. Med.* 2004; 52(6): 1358–1382.
- Sun SW, Song SK, Harms MP, Lin SJ, Holtzman DM, Merchant KM, Kotyk JJ. Detection of age-dependent brain injury in a mouse model of brain amyloidosis associated with Alzheimer's disease using magnetic resonance diffusion tensor imaging. *Exp. Neurol.* 2005; 191(1): 77–85.
- Stejskal EO, Tanner JE. Spin diffusion measurements: Spin echoes in the presence of a time-dependent field gradient. *J. Chem. Physics* 1965; 42: 288–292.
- Helmer KG, Dardzinski BJ, Sotak CH. The application of porous-media theory to the investigation of time-dependent diffusion in *in vivo* systems. *NMR Biomed.* 1995; 8: 297–306.
- Pfeuffer J, Fogel U, Dreher W, Leibfritz D. Restricted diffusion and exchange of intracellular water: theoretical modelling and diffusion time dependence of 1H NMR measurements on perfused glial cells. *NMR Biomed.* 1998; 11(1): 19–31.
- Segebarth C, Belle V, Delon C, Massarelli R, Decety J, Le Bas J-F, Decorps M, Benabid AL. Functional MRI of the human brain: Pre-dominance of signals from extracerebral veins. *NeuroReport* 1994; 5: 813–816.
- Horsfield MA, Barker GJ, McDonald WI. Self-diffusion in CNS tissue by volume-selective proton NMR. *Magn. Reson. Med.* 1994; 31(6): 637–644.
- Nair G, Tanahashi Y, Low HP, Billings-Gagliardi S, Schwartz WJ, Duong TQ. Myelination and long diffusion times alter diffusion-tensor-imaging contrast in myelin-deficient shiverer mice. *NeuroImage* 2005; 28(1): 165–174.
- Merboldt KD, Hancic W, Frahm J. Diffusion imaging using stimulated echoes. *Magn. Reson. Med.* 1991; 19(2): 233–239.
- Bammer R. Basic principals of diffusion-weighted imaging. *Eur. J. Radiol.* 2003; 45: 169–184.
- Reese TG, Heid O, Weisskoff RM, Wedeen VJ. Reduction of eddy-current-induced distortion in diffusion MRI using a twice-refocused spin echo. *Magn. Reson. Med.* 2003; 49(1): 177–182.
- Parker GJM, Wheeler-Kingshott CAM, Barker GJ. Estimating distributed anatomical connectivity using fast marching methods and diffusion tensor imaging. *IEEE Trans. Med Imag.* 2002; 21(5): 8.
- Brockstedt S, Thomsen C, Wirestam R, Holtas S, Stahlberg F. Quantitative diffusion coefficient maps using fast spin-echo MRI. *Magn. Reson. Imaging* 1998; 16(8): 877–886.
- Gullmar D, Hauesien J, Reichenbach J. Analysis of b-value calculations in diffusion weighted and diffusion tensor imaging. *Concepts in Magn. Reson. Part A* 2004; 25(1): 53–66.
- Gullmar D, Jaap T, Bellemann ME, Hauesien J, Reichenbach JR. DTI measurements of isotropic and anisotropic media. *Biomed. Tech. (Berl.)* 2002; 47 (Suppl 1 Pt 1): 420–422.
- Mattiello J, Basser PJ, Le Bihan D. The b matrix in diffusion tensor echo-planar imaging. *Magn. Reson. Med.* 1997; 37(2): 292–300.
- Neeman M, Freyer JP, Sillerud LO. A simple method of obtaining cross-term-free images for diffusion anisotropy studies in NMR micro-imaging. *Magn. Reson. Med.* 1991; 21: 138–143.
- Le Bihan D, Mangin JF, Poupon C, Clark CA, Pappata S, Molko N, Chabriat H. Diffusion tensor imaging: concepts and applications. *J. Magn. Reson. Imaging* 2001; 13(4): 534–546.
- Alexander AL, Hasan K, Kindlmann G, Parker DL, Tsuruda JS. A geometric analysis of diffusion tensor measurements of the human brain. *Magn. Reson. Med.* 2000; 44: 283–291.
- Olah L, Wecker S, Hoehn M. Secondary deterioration of apparent diffusion coefficient after 1-hour transient focal cerebral ischemia in rats. *J. Cereb. Blood Flow Metab.* 2000; 20: 1474–1482.
- Neuvonen T, Salli E. Characterizing diffusion tensor imaging data with directional entropy. *Proceedings of the IEEE Engineering in Medicine and Biology Society*, 2005.
- Jiang H, van Zijl PCM, Kim J, Pearlson GD, Mori S. DTIStudio: Resource program for diffusion tensor computation and fiber bundle tracking. *Comput. Meth. Program. Biomed.* 2006; 81: 106–116.
- Sun SW, Neil JJ, Song SK. Relative indices of water diffusion anisotropy are equivalent in live and formalin-fixed mouse brains. *Magn. Reson. Med.* 2003; 50(4): 743–748.
- Guilfoyle DN, Helpert JA, Lim KO. Diffusion tensor imaging in fixed brain tissue at 7.0 T. *NMR Biomed.* 2003; 16(2): 77–81.
- D'Arceuil HE, Westmoreland S, de Crespigny AJ. An approach to high resolution diffusion tensor imaging in fixed primate brain. *NeuroImage* 2007; 35(2): 553–565.
- D'Arceuil H, de Crespigny A. The effects of brain tissue decomposition on diffusion tensor imaging and tractography. *NeuroImage* 2007; 36(1): 64–68.
- Blamire AM, Rowe JG, Styles P, Mc Donald B. Optimising imaging parameters for *post mortem* MR imaging of the human brain. *Acta Radiologica* 1999; 40: 593–597.
- Pfefferbaum A, Sullivan EV, Adalsteinsson E, Garrick T, Harper C. Postmortem MR imaging of formalin-fixed human brain. *NeuroImage* 2004; 21: 1585–1595.
- Kim S, Chi-Fishman G, Barnett AS. C.P. Dependence on diffusion time of apparent diffusion tensor of *ex vivo* calf tongue and heart. *Magn. Reson. Med.* 2005; 56(6): 1387–1386.
- Assaf Y, Basser PJ. Composite hindered and restricted model of diffusion (CHARMED) MR imaging of the human brain. *NeuroImage* 2005; 27(1): 48–58.
- Yoshiura T, Wu O, Zaheer A, Reese TG, Sorensen AG. Highly diffusion-sensitized MRI of brain: Dissociation of gray and white matter. *Magn. Reson. Med.* 2001; 45(5): 734–740.
- Staempfli P, Jaermann T, Crelier GR, Kollias S, Valavanis A, Boesiger P. Resolving fiber crossing using advanced fast marching tractography based on diffusion tensor imaging. *NeuroImage* 2006; 30.
- Quirk JD, Bretthorst GL, Duong TQ, Snyder AZ, Springer CS Jr, Ackerman JJ, Neil JJ. Equilibrium water exchange between the intra- and extracellular spaces of mammalian brain. *Magn. Reson. Med.* 2003; 50: 493–499.